INSTITUTE OF PHYSICS PUBLISHING JOURNAL OF NEURAL ENGINEERING
J. Neural Eng. **2** (2005) S105–S120 doi:10.1088/1741-2560/2/1/012

Design of a high-resolution optoelectronic retinal prosthesis

Daniel Palanker[1], Alexander Vankov[1], Phil Huie[1] and Stephen Baccus[2]

[1] Department of Ophthalmology and Hansen Experimental Physics Laboratory, Stanford University, Stanford, CA 94305-4085, USA
[2] Department of Neurobiology, Stanford University, Stanford, CA 94305-4085, USA

E-mail: palanker@stanford.edu

Received 11 November 2004
Accepted for publication 14 December 2004
Published 22 February 2005
Online at stacks.iop.org/JNE/2/S105

Abstract
It has been demonstrated that electrical stimulation of the retina can produce visual percepts in blind patients suffering from macular degeneration and retinitis pigmentosa. However, current retinal implants provide very low resolution (just a few electrodes), whereas at least several thousand pixels would be required for functional restoration of sight. This paper presents the design of an optoelectronic retinal prosthetic system with a stimulating pixel density of up to 2500 pix mm^{-2} (corresponding geometrically to a maximum visual acuity of 20/80). Requirements on proximity of neural cells to the stimulation electrodes are described as a function of the desired resolution. Two basic geometries of sub-retinal implants providing required proximity are presented: perforated membranes and protruding electrode arrays. To provide for natural eye scanning of the scene, rather than scanning with a head-mounted camera, the system operates similar to 'virtual reality' devices. An image from a video camera is projected by a goggle-mounted collimated infrared LED-LCD display onto the retina, activating an array of powered photodiodes in the retinal implant. The goggles are transparent to visible light, thus allowing for the simultaneous use of remaining natural vision along with prosthetic stimulation. Optical delivery of visual information to the implant allows for real-time image processing adjustable to retinal architecture, as well as flexible control of image processing algorithms and stimulation parameters.

(Some figures in this article are in colour only in the electronic version)

1. Introduction

As the population ages, age-related vision loss from retinal diseases is becoming a critical issue. Two retinal diseases are the current focus of retinal prosthetic work: retinitis pigmentosa (RP) and age-related macular degeneration (AMD). In these diseases, the 'imaging' photoreceptor layer of the retina degenerates, yet the 'processing circuitry' and 'wiring' subsequent to photoreceptors are at least to some degree preserved. Retinitis pigmentosa occurs in about 1 out of 4000 live births, corresponding to 1.5 million people worldwide. This disease is the leading cause of inherited blindness. Age-related macular degeneration is the major cause of vision loss in people over 65 in the Western world. Each year 700 000 people are diagnosed with AMD, and 10% of these people become legally blind. Currently, there is no effective treatment for most patients with AMD and RP. However, if one could bypass the photoreceptors and directly stimulate the inner retina with visual signals, one might be able to restore some degree of sight.

One important factor affecting this strategy is that the absence of normal signaling from photoreceptors can lead to some progressive degeneration and mis-wiring of retinal circuitry [1, 2]. This type of degeneration is a general property of neural circuits. Thus, for an electronic implant to properly transmit visual signals to the inner retina, any degeneration of circuitry must not drastically change how these signals are interpreted by the higher brain. This is true in the case of cochlear implants, which bypass degenerated primary auditory sensory neurons; both the nerve and the downstream neural

circuitry retain the ability to transmit interpretable auditory information.

Indeed, some first steps have been taken toward the development of an electronic retinal implant. It has been demonstrated that degenerated retina can respond to patterned electrical stimulation in a manner consistent with form vision [3–6]. Human patients implanted with an array of 16 (4×4) electrodes of 0.4 mm in size can recognize reproducible visual percepts with patterned stimulation of the retina [3–6]. The patterns perceived by the patients did not always geometrically match the stimulation pattern, which is not surprising knowing the complexity of the retinal spatial organization. However, the one-to-one correspondence between the perceived and the stimulation patterns gives hope that with some learning and image processing the patients might be able to perceive useful visual information from this type of stimulation [7].

A large percentage of patients with age-related macular degeneration (AMD) preserve visual acuity in the range of 20/400 and retain good peripheral vision. Implantation would be worth its risk for such patients only if it provided substantial improvement in visual acuity. In contrast, patients with advanced retinitis pigmentosa would benefit little unless there was enlargement of the central visual field enough to allow reasonable ambulation. Normal visual acuity (20/20) corresponds to an angular separation of lines by 1 min [8], which corresponds to spatial separation on the retina of about 10 μm, or in other words, spatial frequency $F = 100$ lines mm^{-1} on the retina. To provide such spatial frequency the stimulus pixels should have a linear pixel density at least twice higher: $P \geqslant 2F$, i.e. two pixels per line. In other words, to resolve two white lines at least one black line should be located in between. Thus the maximal spacing between pixels that will allow for resolving two lines separated by 10 μm is 5 μm. Similarly, spatial resolution corresponding to visual acuity of 20/400 corresponds to a pixel spacing of about 100 μm, while acuity of 20/80 (enough for reading with some visual aids) requires pixels smaller than 20 μm, as exemplified in table 1. For these estimates, it is understood that retinal stimulation by one electronic pixel may not produce a perceptual pixel-like 'phosphene', and may generate more complex perceptions dependent on the precise number and connections of stimulated cells. What is essential in this analysis is the fact that pixel density determines maximal amount of information or maximal spatial resolution that can be provided by the stimulating array, and thus the best possible visual acuity, if the brain will be able to utilize all this information. Encoding of the information, i.e. conversion of the image from the video camera into the map of stimulating signals is a separate issue.

It has been previously estimated that 625 pixels can suffice for minimally resolving images in a tiny (1.7° or less) central field [9]. For functional restoration of sight a retinal implant should ideally cover a larger field of view, up to 10° (3 mm in diameter), and support a visual acuity of at least 20/80 (corresponding to a pixel size of 20 μm and density of 2500 pix mm^{-2}) in the central 2–3° of stimulating area.

Electrical stimulation of neural cells in the retina has been achieved with an array of electrodes positioned on either the inner [5, 9, 10] or outer side of the retina [11–13]. Setting the electrodes into the sub-retinal space so as to stimulate bipolar cells, although surgically challenging, has the potential advantage that signal processing in the retina is partially preserved. Full utilization of this advantage will probably require intervention at relatively early stages of retinal degeneration, before significant remodeling of the retinal neural network takes place [2]. Exciting the ganglion cells with electrodes positioned on the epiretinal side abandons the visual processing by the inner retinal network directly stimulating the output of the retinal circuitry.

Table 1. Geometrical approximation of the number of stimulating pixels required for various sizes of the visual field at various levels of visual acuity. The rounded values provide an estimate of the number of square pixels fitting on discs of 1.5, 3 and 6 mm in diameter.

Acuity (pixel size (μm))		Visual field		
		5° (1.5 mm)	10° (3 mm)	20° (6 mm)
20/20	(5 μm)	71 000		
20/40	(10 μm)	18 000	71 000	
20/80	(20 μm)	4 400	18 000	71 000
20/200	(50 μm)	700	2 800	11 000
20/400	(100 μm)	180	700	2 800

One concern with either technique, pertaining to the goal of high-resolution stimulation, is that the electrodes will always be some distance from the target cells. This occurs because the inner limiting membrane and nerve fiber layer intervene in the case of epiretinal approach, or because of photoreceptor remnants in the case of sub-retinal implantation. In addition, diseased retina may have an uneven thickness or wavy structure. Large distances between the cells and closely spaced electrodes result in cross-talk between neighboring electrodes, and the need for a high charge density and power for cell stimulation. This, in turn, can lead to erosion of electrodes and excessive heating of the tissue. Furthermore, any variability in the distance between electrodes and cells in different parts of the implant will result in variations of the stimulation threshold, making it necessary to adjust the signal intensity in each pixel. As shown below [14] for chronic stimulation with pixel density of 400 pix mm^{-2}, which geometrically corresponds to visual acuity of 20/200, the electrodes need to be within 15–20 μm of the target neurons. For visual acuity of 20/80, the separation between electrodes and target cells should not exceed 7 μm [14, 15]. Thus, ensuring a close proximity of cells to the electrodes is one of the most important unresolved issues in the design of a high-resolution retinal prosthesis. In this paper, we describe several techniques that may assure proximity of electrodes to the target cells. One of these techniques prompts migration of retinal cells into proximity of stimulating electrodes positioned in the sub-retinal space [16]. During migration the cells preserve axonal connections to the rest of the retina thus maintaining the signal transduction path. Another technique is based on an array of electrodes protruding from the sub-retinal chip [15].

A very significant problem with current designs of visual prosthetic systems is that they include head-mounted cameras

linked (wirelessly) to the pixels on the patient's retina (Second Sight Inc. [6, 7], EPIRET project [17], MIT-Harvard group [3]), so that eye movements are dissociated from vision. This dissociation compromises greatly the process of natural viewing. When the eye scans a scene, each movement is coupled to a strong expectation that the image will change accordingly. In addition, small eye movements during fixation are actually required for image perception: if an image is stabilized on the retina, it fades from perception within 100 ms [18]. Different approaches based on retinal chips that convert the natural image on the retina into electric signals (Optobionics Inc. [19], Retina Implant AG [20]) do preserve the visual effects of eye movements. However, these systems are limited to (a) bright illumination conditions and (b) have no flexibility in image processing algorithms, which might be essential to compensate for lost image processing in the retina. In this paper, we describe the design of a system with a microcomputer-assisted interface and direct optical projection of the processed image onto photosensitive pixels in the retinal implant using near-infrared light. This system should allow for natural eye scanning and enable the simultaneous use of implant-stimulated vision and any remaining normal vision at any level of luminance.

Another important aspect of macular chip design is adjustable image processing. Synaptic connections from foveal photoreceptors radiate out to bipolar and ganglion cells at some distance from the visual center. Thus, an image centered on the foveola will be processed by bipolar and ganglion cells in a circular zone outside foveola. Prosthetic chips will need to have stimulus signals that match this neural anatomy. The system described below includes location-dependent image processing based on a precise tracking system that monitors the location of the implant in real time. Stimulation of neurons by the retinal implant differs from natural retinal signal processing. Therefore, to enable the translation of stimulus patterns into the conscious recognition of objects, visual chips may require some form of image processing and neural 'learning', much as is required by modern cochlear implants. Tracking the implant in real time allows for the position-dependent image processing that may be required to translate visual information into electrical signals that can be properly interpreted by the higher brain.

In the paper below we describe a system that addresses all three issues raised above: (a) proximity of electrodes to the target cells, (b) delivery of information associated with the natural eye movements, and (c) location-dependent image processing.

2. Physical limitations

In this section, we evaluate the physical constraints that limit spatial resolution of electrical stimulation of the retina as a function of the distance between electrodes and cells. As described in the introduction, for functional restoration of sight an array should ideally cover at least 10° of the visual field (3 mm on retina), and support a visual acuity of at least 20/80 in the central 2–3°. Since peripheral vision has lower visual acuity, the pixel density could, in principle, decrease radially. However, because surgical localization of a chip during implantation may have a degree of uncertainty, and the critical stimulation areas may involve dense arrays of bipolar or ganglion cells in the parafovea, it may be desirable to preserve a high pixel density within much of the disc. It is also expected that functional vision will be easier to achieve if the number of stimulating elements is not at the minimum level. For example, the pixel size corresponding geometrically to a visual acuity of 20/80 is 20 μm, a density of 2500 pix mm^{-2}, which in a 3 mm chip would amount to 18 000 pixels. Chronic stimulation of retina by such a large number of electrodes faces significant technical and biological problems, which we discuss below.

2.1. Voltage and current required for cell stimulation

It is likely that extracellular stimuli will be transduced by bipolar and ganglion cells somewhat differently. Brief ($<$1 ms) capacitive depolarization of the ganglion cell soma opens voltage-gated sodium channels, leading to an action potential, a regenerative propagating ionic current that then travels down the axon. Although bipolar cells typically do not produce action potentials, voltage-gated sodium channels are present in the dendrites and soma [21]. These channels produce fast sodium currents that appear to amplify signal transmission from bipolar cell dendrite to axon terminal [22], analogous to their role in ganglion cells. In addition, extracellular stimulation of bipolar cells will also likely activate voltage-gated calcium channels. These channels have extremely fast kinetics and are present mainly at the synaptic terminals and partially at the soma. In response to depolarization, these calcium channels open and lead to bipolar cell synaptic release in less than 1 ms [23–25].

Numerical simulations of electrical stimulation of retinal ganglion cells have demonstrated that stimulation threshold of the cell body (soma) is slightly lower than axonal stimulation [26]. However, this difference was found to be rather insignificant—less than a factor of 2 [26], which has recently been confirmed experimentally for cathodal stimulation [27]. Based on these findings we have analyzed a simple passive model of extracellular stimulation [28] of the cell body, which allows for analytical solutions, and thus markedly simplifies assessment of various electrochemical and thermal effects.

The typical resting potential of retinal neurons is in the range of 50–70 mV [29, 30], and depolarization of the cell membrane by 5–25 mV is sufficient to transmit a signal to other neurons, including from the graded potential neurons such as bipolar cells [31, 32]. In order to achieve this level of cross-membrane depolarization with extracellular stimulation, a cross-cellular potential is typically induced by application of an electric field to the surrounding medium. Since the impedance of the cellular membrane is much higher than that of the cellular cytoplasm, the interior of a cell quickly polarizes ($t < 1$ μs [33]), i.e. its cytoplasm becomes equipotential so that the trans-membrane potential is increased (hyperpolarized) on the anode side of the cell and similarly decreased (depolarized) on the cathode side [28], as shown in figure 1. In order to achieve depolarization of the cell membrane (reduction of the

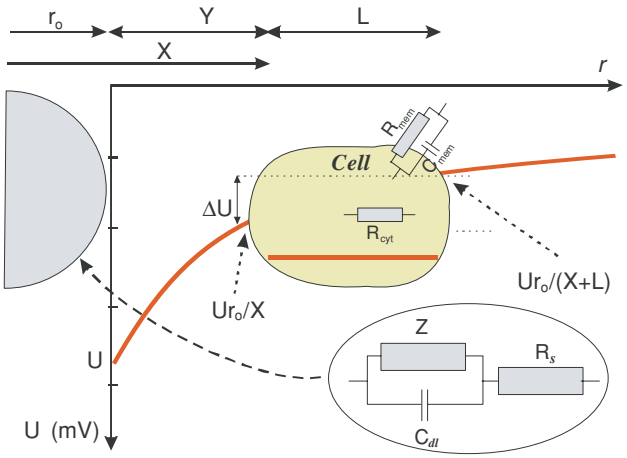

Figure 1. Schematic representation of a cell of the width L positioned on distance X from the center of a hemispherical electrode with radius r_0, (distance Y from its surface). The cross-cell voltage is ΔU. The electrode–liquid interface is shown in the inset. It includes a capacity C_{dl}, faradaic impedance Z, and ohmic resistance of solution R_s.

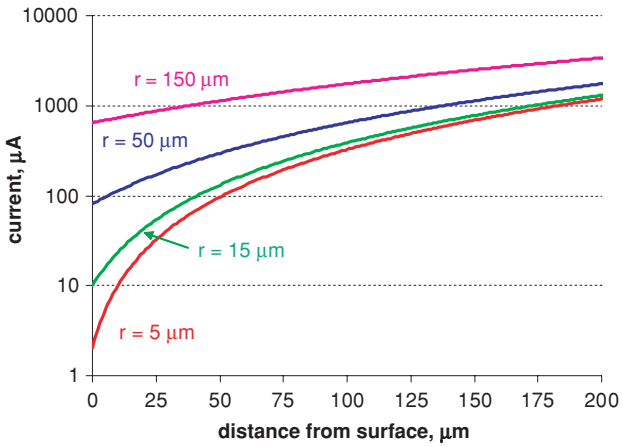

Figure 2. Threshold current required to generate a 30 mV voltage drop across a 10 μm long cell, plotted as a function of distance between the cell and the electrode surface. Calculated for electrode radii of 5, 15, 50 and 150 μm.

trans-membrane potential) by 15 mV [26, 28] the cross-cellular voltage should be twice this amount (i.e. $\Delta U = 30$ mV) in the case of a uniform field. In a non-uniform field, as produced by a small electrode, the trans-membrane potential at the proximal wall will be higher than at the distal wall, with the precise difference depending on cell geometry. Since the membrane depolarizes on the cathode side and hyperpolarizes on the anode side, cathodic stimulation is more efficient with a non-uniform electric field [27]. Approximation of a uniform field in proximity of the cell provides an upper estimate for the threshold potential needed for cellular stimulation.

To achieve a cross-cellular potential of 30 mV in a 10 μm long cell an electric field ofabout 30 V cm^{-1} is required, which will generate a current density of $j = 0.4$ A cm^{-2} in physiological medium with resistivity of 70 Ω cm. Retinal neurons with graded responses, such as bipolar cells, are often depolarized by the stimulus for a more prolonged period of time, and could in theory be depolarized with very long pulses on the order of 1 s. However, long pulses of direct current generate electrochemical reactions at the electrode–electrolyte interface that would lead to an accumulation of chemical products and corrosion. To avoid these effects retinal stimulation systems use pulsed bi-phasic depolarization with pulse durations on the order of $\tau = 0.5$ ms/phase [12, 34, 35]. Charge density delivered with one such pulse can be estimated as $q = j \cdot \tau = 0.2$ mC/cm^2/phase.

The electric field in the medium strongly depends on electrode geometry. Electrodes with sharp features generate uneven electric fields that are greater in areas with small radii of curvature. For example, the electric field at the edges of a flat disc electrode is strongly enhanced [36]. The field becomes relatively uniform only at a distance away that is larger than the radius of the electrode. The use of electrodes with non-uniform fields could make the stimulation of neural cells unpredictable and unreliable, especially if the cells are very close to the electrode.

We model stimulation of neural cells using a hemispherical electrode of radius r_0, which has no sharp boundaries and thus produces a uniform field without singularities, as shown in figure 1, and having a large return electrode at infinity. The current density on the surface of the electrode j_e required to create a voltage drop of ΔU across a cell of length L (measured along the field lines) separated from the surface of electrode by distance Y is [14]

$$j_e = \frac{E_e}{\gamma} = \frac{\Delta U}{\gamma \cdot L}\left(1 + \frac{L}{r_0} + \frac{Y^2 + Y(2r_0 + L)}{r_0^2}\right) \qquad (1)$$

where γ is the resistivity of the physiological solution (e.g. $\gamma = 70$ Ω cm for saline). The required current is minimal when a cell is touching the electrode, i.e. when $Y = 0$. The minimal threshold voltage and current both decrease with radius of electrode, however, if it becomes much smaller than the cell, the electric field will be concentrated in a small area in the proximity of the electrode, while the rest of the cell membrane will not be affected. Thus the optimal size of the electrode designed for selective stimulation of a single cell should be comparable to the cellular size ($L \approx 10$ μm), i.e. its radius r_0 should be about 5 μm. For these sizes of cell and electrode, the stimulating current $I = 2$ μA and corresponding electrode current density $j_e = 1.3$ A cm^{-2}. If the stimulus pulses are of 0.5 ms duration, the corresponding charge density will be 0.65 mC cm^{-2}.

As shown in equation (1), the threshold current required for stimulation of a neuron depends strongly on the size of the electrode and on the distance between the electrode and the cell. As shown in figure 2, the lowest current (2 μA) is required by the smallest electrode size ($r_0 = 5$ μm) when the cell is in contact with its surface, but it increases by an order of magnitude when the cell is separated from this electrode by just 25 μm. The larger electrodes require higher threshold current, but are more tolerant to changes in the separation distance, i.e. the threshold potential does not rise as rapidly with distance as for smaller electrodes. For example, if we define the 'tolerance range' as a distance over which the threshold potential changes

Table 2. Comparison of experimental and theoretical data on threshold charge density required for retinal stimulation. Calculations were performed for a 10 μm cell located in contact with electrode and at distance of half of its radius, as an estimate of experimental conditions.

Reference	Setup	Electrode size (μm)	Pulse duration (ms)	Threshold current (μA)	Threshold charge (μC)	Observed threshold charge density (mC cm^{-2})	Predicted threshold in contact (mC cm^{-2})	Predicted threshold at distance $r/2$ (mC cm^{-2})
Humayun [5]	Epiretinal, human	400	2.0		0.4–0.6	0.32–0.48	0.23	0.62 (at 100 μm)
Rizzo *et al* [3]	Epiretinal, human	100	0.25			0.28–2.8	0.26	0.55 (at 25 μm)
Hesse *et al* [34]	Epiretinal, cat	100	0.4	35–50		0.14–0.20	0.26	0.55 (at 25 μm)
Schwahn *et al* [35]	Sub-retinal, rabbit, pig	100	0.4		0.007–0.05	0.09–0.64	0.26	0.55 (at 25 μm)
Greenberg *et al* [37]	Epiretinal, amphibian, *in vitro*	50	0.1	71	0.007	0.36	0.31	0.60 (at 12.5 μm)
Stett *et al* [12]	Sub-retinal, Chicken, *in vitro*	10	0.5			0.50–0.88	0.64	1.12 (at 2.5 μm)

by a factor of 2, it is only 3 μm for an electrode radius of 5 μm, and 65 μm for the electrode radius of 150 μm. If the distance between electrodes and cells varies for different parts of the array, the stimulation threshold (and the visual outcome) will vary accordingly. Close and stable proximity of cells to the electrodes is thus an important issue in the design of a high-resolution retinal implant.

It has recently been verified experimentally that the dependence of threshold stimulation current on distance between electrode and the cell body is very close to a quadratic (power ≈ 2 in 'Z measurements on cell body', figure 7 in [27]) for distances much larger than the cell body. For small distances this dependence was less steep [27]. Both of these observations fit very well our equation (1). Comparison of the calculated threshold charge densities with published experimental values [4, 5, 12, 34, 35, 37] is shown in table 2 for electrodes not smaller than the cell soma. Comparing the data taken at various pulse durations, we presumed that the strength–duration relationship of the stimulus could be approximated by the charge conservation rule [38]. Theoretical estimates are given for a 10 μm cell located at the electrode and at distance equal to half of the electrode radius, as an estimate of the range of experimental conditions. As one can see from this table, our theoretical estimates are very close to experimental values obtained with various animal species and in humans with several different types of electrodes, and different detection techniques.

2.2. Cross-talk between electrodes

One of the reasons for degradation of resolution when cells are separated from the stimulus electrodes is cross-talk between neighboring stimulus pixels, i.e. the stimulation of one cell by a few neighboring electrodes. Assuming that the dynamic range of prosthetic stimulation should be similar to the range of depolarization voltage under natural conditions, which is greater than 10 dB [31, 32], the interference from the neighboring electrode should be less than 1/10th of the local

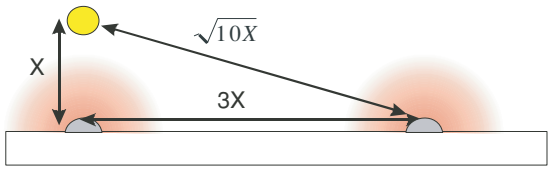

Figure 3. Diagram of the electric fields produced by two neighboring electrodes, and affecting a cell located at distance X in front of one of them.

electric field. Thus, for a cell located at distance X from the primary electrode as in figure 3, the electric field from a neighboring electrode will be 10 times lower if separation between the centers of the electrodes is $3X$ (electric field $E \propto 1/R^2$, and $R^2 = x^2 + (3x)^2 = 10x^2$). This minimal distance ($3x$) between pixels determines the maximal pixel density $n = 1/(3x)^2$, which limits the number of pixels on an array. This effect is similar to taking a picture out of focus: if the CCD array is located out of focus the higher spatial frequencies of the image are 'washed out', and thus lower pixel density is required to transmit the remaining amount of information. Sampling the blurred image with higher pixel density cannot restore the information lost due to the blurring. Figure 4 shows the maximal pixel density as a function of distance between the electrodes and cells determined by the cross-talk. Horizontal dashed lines indicate pixel densities corresponding (geometrically) to various levels of visual acuity. For example, to operate 2500 pix mm^{-2} (visual acuity 20/80) the separation of cells from electrodes (Y) should not exceed 7 μm (1/3 of the pixel spacing). If the cells are 50 μm away, cross-talk would limit the array to only 44 pix mm^{-2}.

2.3. Electrochemical limitations

Current across an electrode/electrolyte interface can be produced by two mechanisms: (i) charging/discharging of the electrical double layer, known as capacitive coupling, and/or

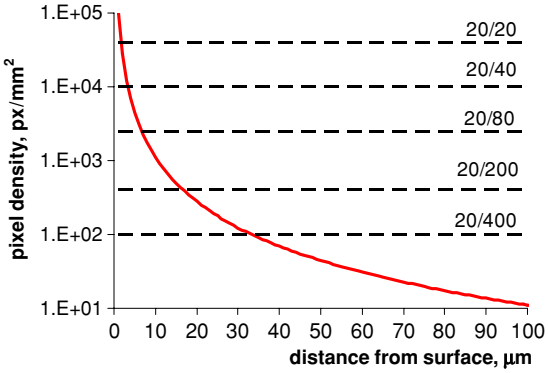

Figure 4. Limit on the pixel density imposed by the cross-talk, plotted as a function of distance between electrodes and cells. Interference level from the neighboring pixels is set to 10% of the primary electric field.

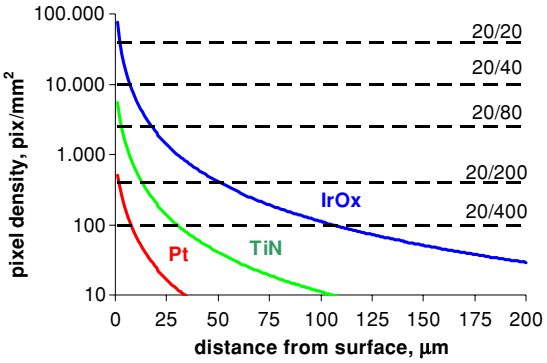

Figure 5. Maximal pixel density as a function of the distance between electrodes and cells. Limits are imposed by maximal charge density on Pt, TiN and IrO_x electrodes.

(ii) electron transfer due to electrochemical reactions at the electrode surface, known as faradaic process. The equivalent scheme of the interface between electrode and electrolyte, illustrating these two paths is shown in the inset in figure 1. It includes the electrical double layer capacitance (C_{dl}) in parallel with the faradaic impedance (Z) [39]. The capacitive coupling between electrode and the medium, i.e. transmission of the current by repetitive charging and discharging of the electrical double layer, has an advantage that it does not involve any electrochemical reactions that could affect the tissue. However, typically the capacitance of the double layer on metal electrodes (on the order of 0.01 mF cm^{-2}) is much lower than what is needed for cellular stimulation. Materials with high surface area, such as carbon black [40] or TiN [41, 42] can, in principle, strongly increase capacitance of the double layer, up to 0.95 mF cm^{-2} [41]. TiN has been reported to have adverse effect on cells in direct contact [43], but this result was not confirmed by a more recent study [42].

Faradaic process can provide higher charge values. However, for chronic stimulation the electrochemical reactions should (a) not cause noticeable decomposition of the electrode material, and (b) its products should not be cytotoxic. Oxidation/reduction of iridium (Ir) oxide on the surface of an Ir electrode satisfies both criteria, and such electrodes have been extensively discussed in the literature [41, 44–46]. Platinum (Pt) electrodes have also been used for cell stimulation [5, 34]. The iridium oxide injects charge by a fast, reversible faradaic reaction involving reduction and oxidation between the Ir^{3+} and Ir^{4+} states of the oxide, with the exchange of charge balancing counter-ions with the electrolyte [46]. Unlike platinum, these redox reactions are confined to the oxide film, with no generation of soluble species required to transfer charge. Accordingly the maximum amount of charge per unit area that can be passed without corrosion for IrO_x electrodes is 4 mC cm^{-2} [41, 45], while for Pt it is much lower: 0.4 mC cm^{-2} [34, 47]. Some studies suggest even more conservative limit of 0.15 mC cm^{-2} [48].

The maximal charge density (current density times pulse duration) determines the minimal radius of the electrode required for 'safe' operation. Assuming that the neighboring electrodes in the array are separated by the three radii of the electrode (the cross-talk limit), the maximal pixel density can be then calculated as $n = 1/(9r_0^2)$. This maximal pixel density is plotted in figure 5 as a function of distance between electrode and cell for Pt, TiN and IrO_x for a pulse duration $\tau = 0.5$ ms and cellular size of 10 μm (see a detailed discussion in [14]). For comparison, we plot on the same graph the pixel densities corresponding geometrically to various levels of visual acuity (horizontal dashed lines). As one can see in this plot, Pt limits the maximal pixel density to about 500 pix mm^{-2} (corresponding to visual acuity of about 20/200), even if cells are in direct contact with electrodes. This number drops to only 17 pix mm^{-2} when cells are separated by 25 μm. Pixel density of 2500 pix mm^{-2} (corresponding to visual acuity 20/80) can be achieved at distances up to 6 μm and 17 μm using the TiN and IrO_x electrodes, respectively.

2.4. Tissue heating

Electrical current in a conductive medium and at the metal/liquid interface generates Joule heat. Heating limits the number of pixels per unit area of an implant because of potential hyperthermia of tissue. With a continuous train of pulses the heat diffusion into the surrounding liquid creates a steady distribution of temperature. Power dissipation from a disk-shaped implant of diameter D surrounded by liquid with thermal conductivity λ having the ambient temperature at infinity is [49] $P_{heat} = 4\,\pi\lambda\,TD$. Assuming the size of an electrode array being $D = 3$ mm, λ being a thermal conductivity of water (0.58 W m^{-1} K^{-1}), and maximal temperature elevation at the implant surface $\Delta T = 1\,^{\circ}$C, results in $P_{heat} \approx 7$ mW. This limit on power dissipation by the implant translates into a limitation on the number of electrodes as a function of distance between them and the cells. As shown in figure 6 for IrO_x electrodes array of 3 mm in diameter (see a detailed discussion in [14]), when the cells are in close proximity to electrodes, the maximal pixel density is limited by packing density rather than by heating. Maximal packing density is estimated assuming the minimal separation between electrodes being equal to radius of the electrode. With electrodes of 5 μm in radius the heating will limit the pixel density at distances larger than 4 μm, and it will be reduced

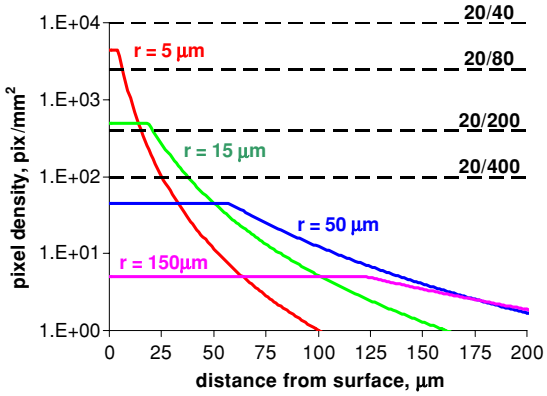

Figure 6. Maximal pixel density in a 3 mm implant to keep heating below 1 °C with 1 ms pulses applied at repetition rate of 50 Hz via IrO_x electrodes. The horizontal segments on each curve represent packing density limit, corresponding to the electrodes separation by a radius.

below the level of 2500 (corresponding to visual acuity of 20/80) at 7 μm. If cells are separated from the electrodes by 50 μm the maximal pixel density drops below the level corresponding to visual acuity 20/400.

2.5. Limits of ambient illumination

One can estimate the maximal intensity of ambient light on the retina when a person is outside in bright sunlight, assuming that he is looking at a highly scattering object, such as a white paper. Irradiance of a direct sunlight $\Phi \approx 100$ mW cm^{-2}, and if it is scattered into the 4π solid angle, the image of this object on retina has the irradiance $J = \Phi \frac{d^2}{16 f^2}$, where d is the pupil diameter, and f is the distance between the ocular lens and the retina. Assuming a pupil size $d = 2$ mm, and $f = 17$ mm [8], the irradiance on the retina will be $J = 0.9$ μW mm^2. With the light-to-current conversion efficiency being <0.8 A W^{-1} a photodiode of 20 μm in size cannot provide more than 40 pA of current.

The irradiance on the retina even under a bright daytime illumination does not exceed 1 μW mm^{-2}. At such illumination a 20 μm diameter photodiode having even 100% quantum efficiency (one photon producing one electron–hole pair) can provide only 40 pA of current. If the light could be accumulated continuously and delivered to the electrodes only during the 0.5 ms 'readout' time at repetition rate of 50 Hz, the current might be increased up to 1.6 nA. However, to provide stimulating current on the order of 1–2 μA, which would be minimal for physiological stimulation, current amplification by a factor of about 1000 is required. Suitable current levels would require photodiodes more than 600 μm in diameter, so that ambient light cannot be used to power more than a token number of electrodes on a retinal chip. An additional source of power will be needed for any practical chip.

3. Attracting retinal cells to electrodes

3.1. Migration of retinal cells into perforated membrane

We have discovered a robust and unexpected property of retinal tissue that promises to reliably and chronically maintain the retina in extremely close proximity to the implant, allowing high-resolution electrical stimulation. In experiments *in vitro*, in which retinas were placed photoreceptor-side down upon the membrane, a robust migration of retinal tissue into small apertures was observed in all samples of the rat, chicken and rabbit retina [16]. Migration of the outer nuclear layer, outer plexiform layer and inner nuclear layer occurred through apertures larger than 5 μm. The cellular invasion of the aperture appeared to include both glial and neural cellular elements, and the rate of tissue migration increased with aperture size. A transmission electron micrograph of a section through an aperture demonstrated the presence of neuronal processes and synaptic structures connecting the migrating cells. These findings indicate the possibility of signal transduction from the stimulated cells to the rest of the retina.

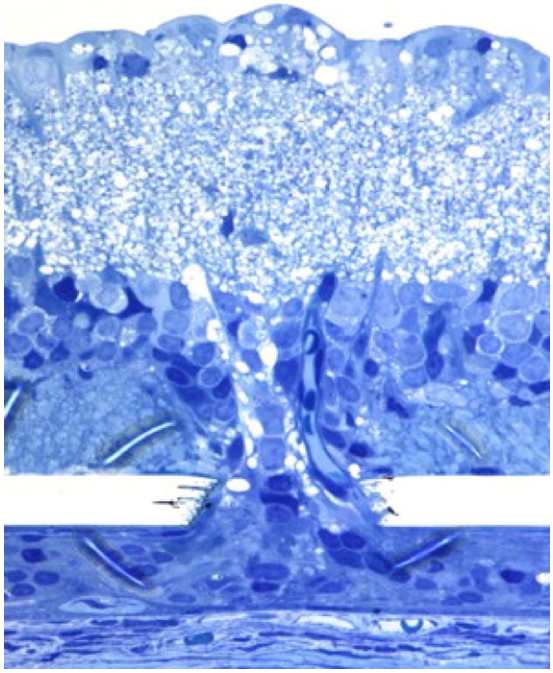

Figure 7. Histological sections of the RCS rat retina 9 days after implantation. Retinal tissue (INL) migrates through the aperture of 40 μm in a 13 μm thick Mylar membrane and spreads above the RPE. Scale bar is 50 μm.

Culturing of the retina upside down (tested on the P7 rat retina), i.e. nerve fiber layer toward the membrane, did not result in cellular migration.

The RCS rat was used as a model for *in vivo* experiments, since the photoreceptors degenerate as in RP experiments with sub-retinal Mylar films perforated with apertures of 15–40 μm in diameter showed robust migration of the inner nuclear layer after 5 and 9 days (figure 7). Since unlimited tissue migration through a membrane could be problematic (draining retinal cells and proliferating under the prosthesis) we explored the placement of perforated membranes with a basal seal to prevent growth out the bottom. These experiments were performed *in vitro* with cultured rat retinas. In the experiment illustrated in figure 10, the 20 μm perforations lay atop a small chamber,

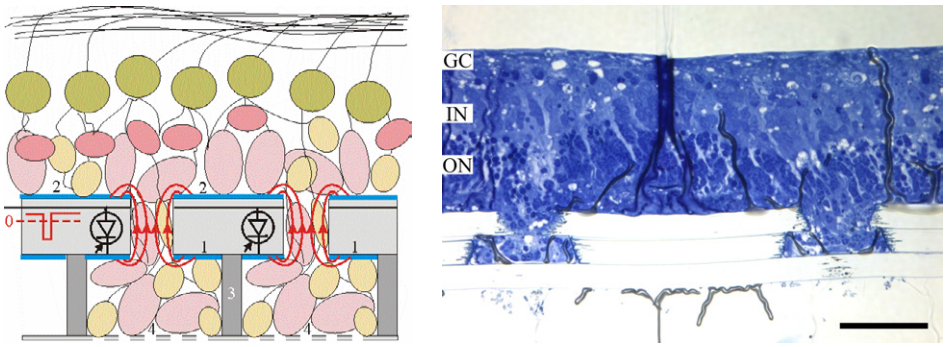

Figure 8. (A) Schematic of a three-layered membrane with entry channels on top, wider inner chambers, and a fenestrated membrane 4 at the bottom. Voltage can be applied between the inner electrode (1) and the common return electrode (2). (B) Rat retina grown on the three-layered structure for 7 days *in vitro*. Retinal cells migrated through the 20 and 35 μm holes into the middle chambers of 60 μm in width, but not through the 3 μm holes in the lower membrane. Scale bar is 50 μm.

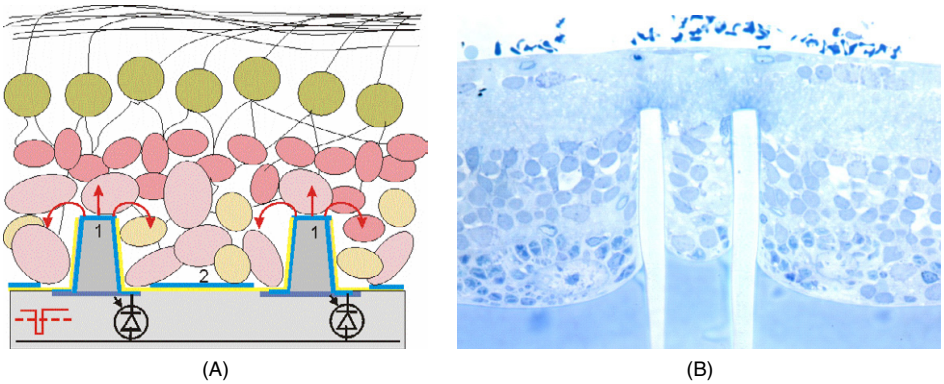

Figure 9. (A) Concept of protruding electrodes on the sub-retinal array penetrating deep into the retina after migration of the retinal cells into the empty spaces between the pillars. Penetration depth is set by the length of the pillars, which are insulated at the sides and exposed at the top. (B) Lithographically fabricated 10 μm wide pillars penetrating into the inner plexiform layer in the retina of RCS rat 15 days after the implantation.

and the bottom was sealed with a membrane having tiny (3 μm) perforations that would pass nutrients but not cells (figure 8(A)). When retinas were cultured over this three-layer structure for 7–14 days, tissue was observed to migrate into the chambers but no further (figure 8(B)).

Major concerns are whether the neural cells that migrate into the pores will survive for an extended period of time, whether the neural circuitry will be disrupted and whether the migrated tissue will change through glial overgrowth or cell death. The long-term behavior of retinal cells migrating into perforated membranes should be further studied to optimize the membrane structure for preserving neural connections and assuring efficacy of an electric interface.

3.2. Migration around protruding electrodes

Another promising technique for providing close proximity between the neural cells inside the retina and the stimulating sites of the implant involves protruding electrodes. As diagrammatically shown in figure 9(A), stimulating electrodes 1 would extend by several tens of micrometers above the surface of photodiodes and be exposed only at the top of the 'pillars', with a common return electrode 2 on the surface of the wafer. This array would be positioned in the sub-retinal space, so that cells could migrate into the empty space between the pillars, similarly to the migration we observed with the perforated membrane. This way the electrodes will penetrate into retina without mechanical stress and associated injury. This technique is complimentary to the perforated membrane in a sense that the cells which do not migrate and thus remain in the depth of retina can be stimulated by the penetrating electrode, as opposed to the perforated membrane, where only the migrating cells that will penetrate into the bottleneck of the chamber can be stimulated. The depth of penetration will be determined by the length of the pillars. The pillars can be manufactured using conventional photolithographic technology. To demonstrate the feasibility of this design, we manufactured an array of pillars of 70 μm in height and 10 μm in diameter using photolithography with SU-8 photoresist. We implanted these arrays into the sub-retinal space in adult rats with retinal degeneration. Histology performed on eyes enucleated 15 days after the implantation is shown in figure 9(B). As one can see in this figure, the retina is well preserved with the inner nuclear layer slightly disturbed by the pillars that penetrated into the inner plexiform layer. Shorter pillars will be used for addressing the inner nuclear layer.

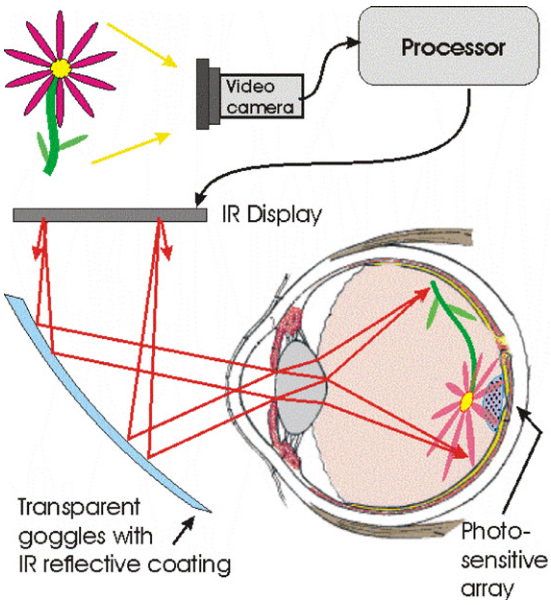

Figure 10. Image projection from the goggles display onto the retina. Part of the image which is projected onto the retinal chip activates its photosensitive stimulating pixels.

4. Delivery of information and power to the implant

4.1. Projection system

The projection system is designed to allow natural eye scanning for image perception, flexibility of image processing between the camera and the implant, and utilize any remaining intact vision. The system controls the stimulating signal in each pixel by projecting light from the goggles display onto a retinal implant with an array of powered photodiodes, as diagrammatically shown in figure 10. An image from the small video camera located on the patient's goggles is processed using a portable microcomputer (pocket PC). The processed image is displayed on the LCD micro-display similar to those used for 'virtual reality' imaging systems (medical, military, etc). The LCD display will emit near-infrared (IR) light (800–900 nm). The IR image from the display is reflected from the transparent goggles and projected onto the retina using natural optical properties of the eye, as shown in figure 10. The projected IR image is thus superimposed onto a normal image of the world observed through the transparent goggles. The retinal chip has an array of photosensitive elements converting the IR light into stimulating current in each pixel using a pulsed bi-phasic power provided by a photovoltaic battery, or otherwise, as described below. Advantages of this system as compared to current approaches to visual prosthesis include the following:

- Transmission of information from the LCD screen to each pixel in the chip is conducted by light simultaneously, i.e. pixels are activated in a parallel fashion, and there is no need for serial decoding in the implant, as it is done for the single emitter–receiver links (either optical [17] or radio frequency [3]).
- The IR video display on the goggles can emit as much power as the eye can thermally tolerate thus providing a robust signal to each pixel at any level of ambient illumination.
- The system's design allows implant-stimulated vision at the same time when residual natural vision of the patient functions normally in the areas outside the retinal implant. The infrared projected image is not detected by normal vision. Conversely, the implant's infrared sensitivity is such that its response to visible light is negligible compared to the bright infrared image. The tracking system that monitors the position of the implant at each moment (described below) will allow for alignment of the stimulated parts of the image and those perceived normally.
- The video display projects an image corresponding to the field of view which is much larger than the retinal chip (typically covering only a small solid angle). With this system, the patient can use his natural eye movements in order to observe the larger field of view, rather than scanning the field of view by moving his head-mounted video cameras.
- Intensity, duration and repetition rate of the stimulating signal produced by the retinal chip can be controlled by the intensity, duration and repetition rate of the light-emitting pixels in the screen. These parameters can be adjusted without need for any changes in the retinal chip itself. This feature provides flexibility in optimization of the stimulation parameters and image processing algorithm, which might have to be adjusted for each patient.
- This projection system can be used for both epiretinal and sub-retinal implants.

As described above, the stimulation current for an electrode of 10 μm in diameter is on the order of 1 μA. The photodiode converts photons into electric current with efficiency of up to 0.6 A W^{-1}, thus 1.7 μW of light power will be required for activation of one pixel. If light pulses are applied for 1 ms at 50 Hz, the average power will be reduced to 83 nW/pixel. With 18 000 pixels on the chip, the total light power irradiating an implant will be 1.5 mW.

LCD screens used in video goggles emit light into a wide angle, and only a small fraction of it (typically $<1\%$) reaches the retina, while most of it is absorbed by the sclera and iris. In addition, only a small part of the retina (about 5%) is covered by an implant which requires high brightness, while peripheral vision can operate at natural (much lower) level of luminance. To provide 2 mW of light on a 3 mm retinal implant, the LCD goggles should in total emit about 4 W of light power! This is certainly not practical.

This problem can be resolved by addressing both aspects of the loss of light: (1) providing a collimated illumination and (2) activating at high brightness only a small part of the screen—which is projected onto the implant, position of which will be constantly monitored with a tracking system (figure 12). The high brightness pulsed illumination for the implant will be provided by the near-IR LED array positioned behind the LCD screen, as shown in figure 11. A condenser lens directs the main axis of the diodes into the center of the eyeball.

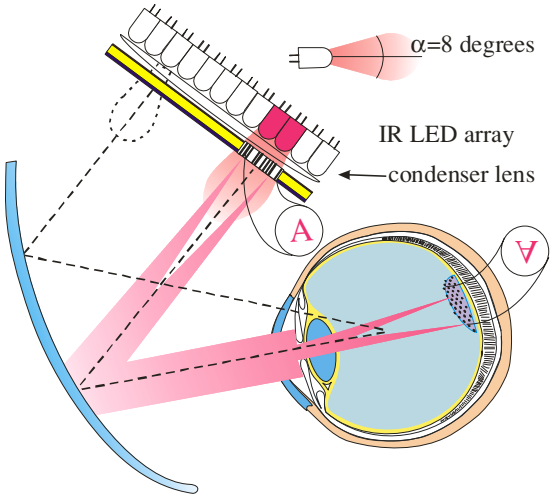

Figure 11. Diagram of the LED array used for collimated illumination of the LCD screen.

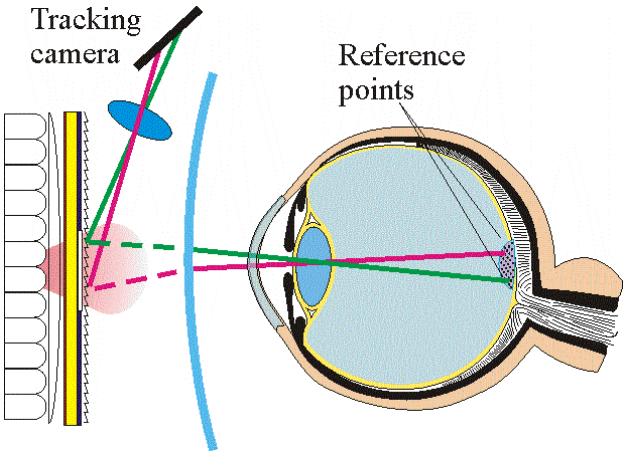

Figure 12. Tracking system monitoring position of a few reference points on the retinal implant. View from above. LCD and tracking camera are above the eye level.

Assuming no magnification between the screen and the retina, the diameter of the light spot on the pupil will be $D = d_{\text{chip}} + \alpha L$, where d_{chip} is the implant size, $\alpha = 8^\circ$ is the divergence of the LED beam, and $L = 17$ mm is the distance between the implant and the pupil. With these assumptions the spot of light on iris will be 5.3 mm in diameter. With the pupil of 3 mm in diameter, 32% of light will be transmitted into the eye, thus only 6 mW of power in the region covering the implant would be required from the LCD screen.

4.2. Location-dependent image processing

The central part of the macula (fovea) does not contain bipolar and ganglion cells. Photoreceptors in this area radiate their synaptic connections outside the fovea (Henle's fibers), to a distance of about 0.5 mm in diameter, as shown in figure 13. Thus if the retinal chip covers the macula, the image should be processed so that stimuli are delivered to the bipolar or ganglion cells outside the foveola. This means that an image projected onto the retinal stimulating array should have a black spot in the foveola (since there are no cells to stimulate in that area), and the rest of the macular area should be stretched in a radial pattern matching the retinal organization in the macula, as shown in figure 13. An example of such image processing is shown in figure 14. The fact that retinal architecture is non-uniform around the center of the macula necessitates image processing that depends on position of the foveola relative to the projected image, i.e. it depends on what part of the field of view the person is looking at.

There are several additional reasons necessitating the position-sensitive image processing for the visual chip controlled by the optical projection system:

- The retina has a complex system of image processing involving intertwined patterns of ON and OFF cells with large receptive fields having center-surround organization. For correct transmission of the image there might be a need for the stimulation pattern matching this cellular organization. In addition, there might be a need for temporal variation of the stimulation of the neighboring pixels [50].
- Part of the retinal implant system might be a photovoltaic cell that generates power for the stimulating array. To generate power at maximal efficiency, the region of the display imaged onto the battery could emit continuous bright light (figure 14).
- Various pixels in the array may have different impedances (due to the tissue growth or electrode contamination) or different distances from the cells and thus may require different pulse characteristics such as intensity or frequency.

Because the image processing between the video camera and the IR LED-LCD array that transfers information to the implant should depend on the position of the implant, a real-time tracking system is required.

4.3. Implant tracking system

Since the eye is frequently moving, fixating on different parts of the image, the proper image processing and activation of the display requires information about the position of the retinal chip at each moment. Therefore, another aspect of the projection system includes a tracking system (figure 12) for the optically activated retinal chip. This system monitors positions of a few reference points on the retinal implant. The reference points reflect or emit light back through the pupil and are imaged onto the tracking array which is positioned in the conjugated plane with the LCD display. For tracking the location and torsional orientation of the retinal chip only two reference points on its surface should be sufficient. More reference points may provide higher reliability and precision in localization of the chip. During fixation, the human eye drifts at an average angular velocity of $0.5^\circ\ \text{s}^{-1}$, up to $2^\circ\ \text{s}^{-1}$ [51]. In contrast, during saccades, large ballistic movements, the eye can move with a velocity of hundreds of degrees per second. However, normal visual perception is greatly decreased during

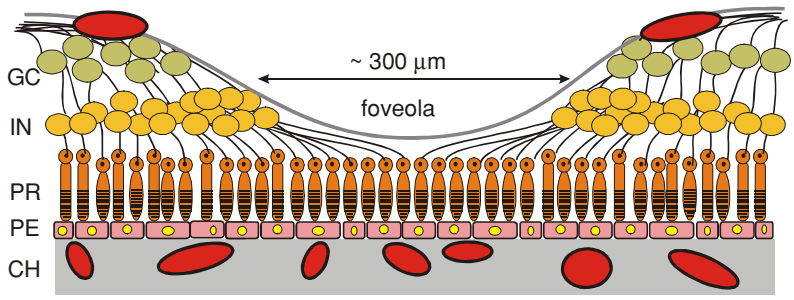

Figure 13. Diagrammatic representation of the human fovea with bipolar and ganglion cells located outside the foveola. Labels of the retinal layers: GC–ganglion cells, IN–inner nuclear, PR–photoreceptors, PE–retinal pigmented epithelium, CH–choroids. Red ovals inside the choroid and above the GC layer are blood capillaries.

Figure 14. Left: a wide view of a scene by the video camera. Right: the same image processed for the position of the macula centered on the right edge of the traffic light. Black spot corresponds to foveola, where no cells will be stimulated. Pixels around the black spot are stretched radially in order to match retinal architecture (lighter circle). A yellow circle indicates a part of the display projected onto a photovoltaic battery located on retina aside the stimulating chip. The rest of the image represents a view through the transparent goggles for the remaining natural vision of the patient.

saccades, especially to motion, so real-time image processing will not be required at these rates.

Reference points on the implant can be made, for example, in the shape of three-sided pyramidal indentations with highly reflective walls, thus reflecting light in the direction of incidence. They also may be made as small LEDs emitting a wavelength or temporal pattern different from that emitted by the image display. This will allow for discrimination between the emission by the reference points and scattering from elsewhere in the eye. To allow for localization of the reference points with a spatial resolution of a half of a pixel in the implant (10 μm) the tracking system should have angular resolution of 0.03°. Thus, the imaging array of the tracking system, having a visual field of 30° should have at least 1000 pixels in a row. Modern video cameras have 1600 × 1200 pixels with a frame rate of 30 Hz, providing a dynamic range of 8 bits (gray scale), which is well suited for this application.

Knowing the current position of the chip and relation of the fovea to the chip, the image on the display will be adjusted appropriately. For example, the pixels in the center of the field of view can be distributed peripherally a few hundred micrometers to accommodate the absence of foveal circuitry, the power supply (photovoltaic cell) will be properly illuminated, and the relative intensities and delays in different pixels will correspond to the required pattern on the chip. Software for this type of real-time image processing is currently under development and testing in our group.

4.4. Optoelectronic implant design

As described above, proximity of retinal cells in the inner nuclear layer to the stimulating electrodes can be achieved by promoting cellular migration into the sub-retinal implant. One possible design of a sub-retinal photosensitive stimulating array that takes advantage of this effect is shown in figure 8(A). A wafer of about 15–25 μm in thickness is divided into separate photosensitive pixels similarly to a CCD array. In each pixel, there is a channel of about 5–15 μm in diameter for cellular migration. Each pixel is a biased photodiode which converts light intensity into bi-phasic charge-balanced pulses. All the pixels are connected to one common bi-phasic power line. The negative phase of the waveform is transmitted through the photodiodes as a function of light intensity. The positive phase passes through the diodes providing compensation for the charge balance. To avoid irreversible electrochemical reactions on IrO_x electrodes, the voltage is limited within the range from −0.6 to +0.8 V, and charge density is limited to 4 mC cm^{-2} [41, 45]. In preliminary experiments with such circuits we verified preservation of the charge balance with precision better than 0.01% independently on the light intensity in individual pixels. The stimulating bi-phasic pulse conducted through the photodiodes is applied

to the inner electrode 1 in the cavity, while the return electrode 2 is transparent and common to all pixels in the array. To form a cavity the wafer is mounted on a spacer layer 3 which is closed on its lower side with a perforated membrane 4 limiting cellular migration but allowing for a flow of nutrients and oxygen. An electric field is applied between electrodes 1 and 2, stimulating the cells located at the 'bottleneck' of the channel, as shown by red arrows in figure 8(A). Alternatively, the addressable electrodes are positioned at the bottom of each chamber, while the upper membrane is a simple perforated insulator with a conductive coating at the top. The semiconductor wafer at the bottom in this case has no perforations and thus its manufacturing is conventional and inexpensive. The current from the lower electrode in each chamber is concentrated inside the aperture in the upper membrane and thus the cells located in and near this bottleneck will be affected by electric field the most. In case the cells inside the chamber do not survive for extended periods of time, cells in the bottleneck will still be stimulated. Furthermore, even if cells in the bottleneck are not functional, the stimulation zone can be extended up and around the aperture by positioning the return electrode slightly away from the edge of the aperture.

An upper estimate of the current, charge density and power dissipation can be given assuming that the cells located in the bottleneck do not increase the electric impedance between electrodes 1 and 2. Impedance of the 15 μm long channel of 10 μm in diameter filled with physiological medium is about 150 kΩ. The charge transfer resistance and the resistance of the oxide layer for IrO_x electrode of 10 μm in radius will add another 50 kΩ. An electric field of 30 V cm^{-1} (threshold for cellular stimulation) corresponds to a current density of 0.4 A cm^{-2}, thus resulting in the total current of about 0.3 μA across this channel. If the maximal signal is 10 times above the threshold value (i.e. 3 μA), the total charge transfer during 0.5 ms pulse will be 1.5 nC. For the inner electrode of 10 μm in radius, the charge density will be about 0.5 mC cm^{-2}, which is well below the safe limit of 4 mC cm^{-2} for an IrO_x electrode [41, 45]. Pseudo-capacitive voltage steps at the electrode–liquid interface will reach 100 mV by the end of each pulse. The heat generated during a 1 ms pulse (two phases of 0.5 ms each) is about 3 nJ. If applied at repetition rate of 50 Hz the average heating power will be 150 nW. Even with 18 000 pixels the average power will not exceed 2.7 mW.

Photodiode conversion efficiency (light-to-current) is typically less than 0.6 A W^{-1}, thus for generation of 3 μA of current about 5 μW of light power will be required in each pixel. For a pixel size of 20 μm this amount of power corresponds to an irradiance of 13 mW mm^{-2}. If pulses of 0.5 ms in duration are applied at 50 Hz the average power density will be 0.31 mW mm^{-2}. For a chip 3 mm in diameter the total average power will thus be 2.2 mW. Together with electrical power estimated above, the total power dissipation at maximal stimulation level (10 times the threshold) on all 18 000 pixels in the implant will be about 5 mW. This corresponds to the temperature rise of 0.7 °C at the surface of the 3 mm disc array. This level of chronic heating at maximal stimulation level seems acceptable. If heating becomes a problem, the repetition rate could be reduced to 25 Hz or even 15 Hz, thus producing 'slower' vision, as occurs in human perception in near darkness. As described above, only the image projected onto the retinal chip will be illuminated brightly with IR light. The rest of retina will receive natural image through transparent goggles.

If, in fact, the bottleneck of a chamber is partially blocked by a cell, increasing the impedance in parallel to the cell, this is actually an advantage because the required voltage drop across the cell will be achieved at a lower current. However, encapsulation of electrodes surfaces with glial layer might be a problem, since this might disconnect the electrodes from the medium, increasing the impedance in series with the cell, requiring a greater voltage to stimulate the cell. Encapsulation might be prevented using coatings that can inhibit glial cell growth and fibrosis [52].

An alternative approach to placing the electrodes in close proximity to the cells using penetrating electrodes is shown in figure 9(A). The biased photodiodes will have lithographically made pillars with a conductive coating extending several tens of micrometers above the wafer. The pillars will be insulated except for the top, where an electrode (1) coated with IrO_x will be exposed. The common return electrode made of a transparent conductive material will cover the rest of the surface of the array (2). The implant positioned into the sub-retinal space induces migration of retinal cells into the spaces between the pillars, thus allowing for pillars to penetrate to the depth determined by their length, as shown in figure 9(B), without forceful insertion and associated mechanical injury.

In this approach, the actively migrating cells will move toward the bottom of the implant while allowing the electrodes to reach the cells which migrate slower or do not migrate at all. The pores and pillars approaches are complimentary: in the first case the actively migrating cells penetrate into the pores and are stimulated. In the second case the migrating cells move toward the bottom of the implant and the electrodes approach the cells which remain in place.

4.5. Resolving problems of the edge effect

Conventional flat metal electrodes have a serious problem with non-uniformity of electric field and associated current density [36]. As shown in figure 15, the field is much stronger at the sharp edges of the flat electrode, where it is enhanced by the ratio of the electrode radius to the thickness of the metal coating. Even with small electrodes this effect is very significant: for example, with electrode radius of 5 μm and thickness of 1 μm, this ratio is close to a factor of 5 (figure 15), and with larger electrodes it becomes even worse. As a result, at the edges the cells will experience fields much higher than in the center, which may lead to a strong pixel-to-pixel variation in stimulation threshold. In addition, high current density at the edges may lead to rapid electrochemical erosion and cellular damage in these areas.

The electric field produced by a porous electrode design, as we have proposed, is much more uniform (figure 15). In addition, because the pore diameter is smaller than the size of electrode inside the pore, the current density on the electrode is much smaller than in the case of the flat metal electrode.

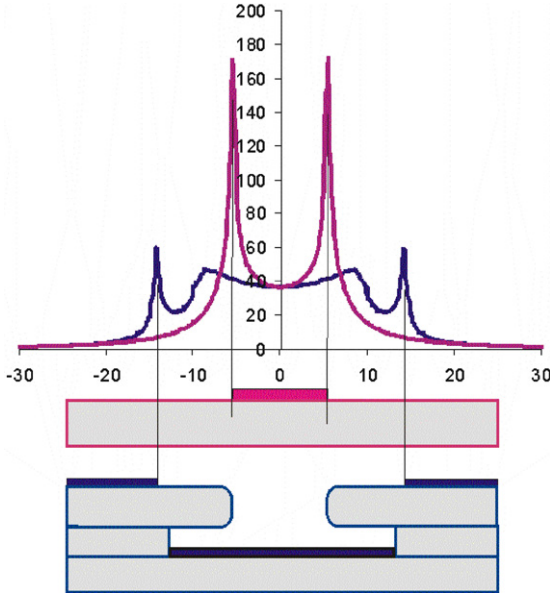

Figure 15. Distribution of electric fields calculated for the flat metal electrode (red) and the pore electrode (blue).

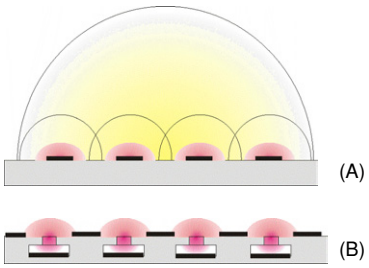

Figure 16. (A) Currents from each electrode add up and produce electric field extending to the distance equal to the size of the implant making local stimulation very difficult. (B) Currents are localized in each pixel between the inner electrodes and the common return electrode at the top of the array, thus the stimulation is selective and local.

For the geometry shown in figure 15, the current density on the metal inside the pore is 12 times lower than that on the flat metal electrode. This design significantly reduces the pseudo-capacitive voltage drop at the metal–liquid interface, thus reducing the heating and potential electrochemical problems.

4.6. Collective effect of multiple electrodes

There is yet another problem with the conventional design of the stimulating implant, i.e. an array of the flat metal electrodes with the large return electrode at infinity. When multiple electrodes are activated simultaneously on such a chip, their currents add up and produce an electric field extending to a distance equal to the radius of the array (typically on the order of millimeter), as shown in figure 16(A). Since the retina is much thinner than the size of the implant all the layers of cells in the retina will be stimulated together in this case, instead of localized stimulation of the target cells.

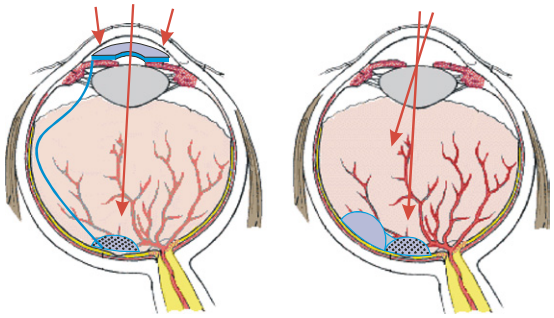

Figure 17. The retinal implant converts an image into the stimulating signal using the energy of the photovoltaic power supply located in the anterior chamber (left) or next to the stimulation array (right).

The design of porous electrodes with the return electrode at the top solves this problem. The local currents in this case are restricted within each pore and do not add up at large distances, as shown in figure 16(B). Thus cells located at each pixel can be stimulated selectively and independently from signals applied to other electrodes.

4.7. Power supply

As described above, the optoelectronic prosthesis having 18 000 pixels and 10 μm electrodes can consume up to 3 mW of power from the bi-phasic power supply. This power can be generated inside the eye with photovoltaic batteries using part of the light projected from the goggles. The most efficient place for collection of the ambient light is the anterior chamber, for example, in front of the iris, as shown in figure 17. The power supply will consist of two segments generating voltages of opposite polarity, and a switching mechanism that will apply bi-phasic pulses to the retinal stimulating array. The implant is a thin (25 μm) wafer with photovoltaic cells and pulse generator encapsulated in a transparent biocompatible coating. As we estimated above, with a pupil of 3 mm in diameter 3 times more power falls on the iris than on the retinal implant, thus providing adequate amount of light for the anterior photovoltaic battery.

Placement of the photovoltaic battery in the anterior chamber, although beneficial from the optical point of view, is surgically challenging since it requires connecting the two independently placed implants (retinal and anterior) with a wire. Alternatively, the photovoltaic battery can be placed on the same implant with the stimulating array, which makes the surgical procedure significantly simpler. In this case, the LED–LCD screen should emit an additional pattern of light projected onto the photovoltaic battery, as shown in figure 14. Since not more than 30% of light energy can be converted into electrical energy, not less than 9 mW of light power should illuminate the battery in order to generate the required 3 mW of electric power. To avoid heating the retina by more than 1 °C, the total power dissipation by the power supply should not exceed 7 mW, and thus the repetition rate of stimulation in the implant might need to be reduced from 50 to 25 Hz. Alternatively, a power supply can be based on RF transmission of energy

from the coil located on the goggles into a coil inside or outside an eye.

5. Advanced signal processing

Since stimulation of neural cells by the retinal implant differs from the natural mechanisms of visual signal processing in the retina, restoring natural sight will require the combination of a number of factors. Perhaps the most important will be plasticity of neural networks that will learn to interpret electrical stimulation of the partially degenerated retina. To minimize the reliance on neural plasticity, it is desirable for the stimulated signals to match as closely as possible natural visual responses. This is most likely if the implant is placed as early in the visual system as possible. In addition, placing the implant early in the visual pathway takes advantage of existing downstream neural processing, and minimizes the necessity of electronically pre-processing the image so as to reproduce the processing of bypassed neural circuitry. In cases of complete photoreceptor degeneration, the earliest point an implant can stimulate is bipolar cell dendrites. Thus, two main aspects of visual processing that would likely be compromised are color processing, which arises by virtue of different cone types, and separation of neural signals into the ON and OFF pathways, which occurs at the photoreceptor–bipolar synapse. Though the absence of color vision would prevent some object discrimination, it would still allow the detection of the presence of objects. As to the ON and OFF pathways, an implant that depolarizes neurons in response to an increase in light intensity would stimulate the ON pathway with the correct sign, but the OFF pathway would receive an inverted signal. However, many visual neurons have rectified responses, responding to either sign, and thus a number of aspects of visual processing might not be substantially affected. For example, many ganglion cells are of the 'ON–OFF' type, responding to either increases or decreases in light intensity. Additionally, in the retinal pathway that distinguishes moving objects from background motion, signals are rectified, and exchanging black for white does not change the firing patterns of object motion sensitive retinal ganglion cells [53].

Advanced processing of the image could potentially restore an even higher level of vision, though these methods would be most affected by the precise level of degeneration of retinal circuitry. Both correct color and contrast processing could conceivably be restored if the visual scene was pre-processed in different ways appropriate to the separate pathways and then addressed separately to those pathways. This becomes possible with a precise tracking system that can detect the location of the implant in real time. In addition, it would require that individual electrodes only communicate with a single channel of contrast (e.g. only ON or only OFF cells). Electrodes of 10 um in size might enable this level of selectivity. Which cell types are, in fact, activated by individual electrodes will be determined in animals by application of various stimulation patterns while recording from ganglion cells with a multielectrode array [54, 55]. In humans this function would be performed based on communication with the patient.

In summary, (a) high enough resolution for useful vision cannot be achieved unless very close proximity (on the order of cellular size) between the electrodes and target cells is established along the whole interface of the implant with the retina; (b) for normal visual perception the image should not be dissociated from the eye movements; and (c) the image processing between the camera and the implant should depend on the implant location, i.e. direction of gaze. The system described in this paper includes (1) an optically controlled implant enabling delivery of visual information related to the natural eye movements, (2) position-sensitive image processing, and (3) techniques for bringing retinal neurons into required proximity with stimulus elements.

Acknowledgments

Authors would like to thank Drs Robert Aramant and Magdalene Seiler from the Doheney Eye Institute at UCSC for their help with sub-retinal implantation into the RCS rats. We also express our appreciation to Professor Michael Mirkin from Queens College at CUNY for consultation on issues of electrochemistry, and to Professors Mark Blumenkranz, Michael Marmor and Dr Harvey Fishman from the Department of Ophthalmology at Stanford for discussions and encouragement. Funding was provided in part by the Medical FEL program (Department of Research at the US Air Force) and VISX Corp.

References

[1] Marc R E and Jones B W 2003 Retinal remodeling in inherited photoreceptor degenerations *Mol. Neurobiol.* **28** 139–47

[2] Marc R E, Jones B W, Watt C B and Strettoi E 2003 Neural remodeling in retinal degeneration *Prog. Retin. Eye Res.* **22** 607–55

[3] Rizzo J F, Wyatt J III, Loewenstein J, Kelly S and Shire D 2003 Perceptual efficacy of electrical stimulation of human retina with a microelectrode array during short-term surgical trials *Invest. Ophthalmol. Vis. Sci.* **44** 5362–9

[4] Rizzo J F, Wyatt J III, Loewenstein J, Kelly S and Shire D 2003 Methods and perceptual thresholds for short-term electrical stimulation of human retina with microelectrode arrays *Invest. Ophthalmol. Vis. Sci.* **44** 5355–61

[5] Humayun M S, de Juan E, Weiland J D, Dagnelie G, Katona S, Greenberg R and Suzuki S 1999 Pattern electrical stimulation of the human retina *Vis. Res.* **39** 2569–76

[6] Humayun M S 2003 *Clinical Trial Results with a 16-Electrode Epiretinal Implant in End-Stage RP Patients* (Fort Lauderdale, FL: Department of Energy) p 10

[7] Humayun M S, Weiland J D, Fujii G Y, Greenberg R, Williamson R, Little J, Mech B, Cimmarusti V, Van Boemel G, Dagnelie G and de Juan E 2003 Visual perception in a blind subject with a chronic microelectronic retinal prosthesis *Vis. Res.* **43** 2573–81

[8] Smith G and Atchison D A 1997 *The Eye. The Eye and Visual Optical Instruments* (Cambridge: Cambridge University Press) pp 291–316

[9] Margalit E *et al* 2002 Retinal prosthesis for the blind *Surv. Ophthalmol.* **47** 335–56

[10] Margalit E *et al* 2003 Visual and electrical evoked response recorded from subdural electrodes implanted above the

visual cortex in normal dogs under two methods of anesthesia *J. Neurosci. Methods* **123** 129–37
[11] Zrenner E *et al* 2001 Subretinal microphotodiode arrays to replace degenerated photoreceptors? *Ophthalmology* **98** 357–63
[12] Stett A, Barth W, Weiss S, Haemmerle H and Zrenner E 2000 Electrical multisite stimulation of the isolated chicken retina *Vis. Res.* **40** 1785–95
[13] Sachs H G, Kobuch K, Koehler M, Schwahn H N, Gekeler F E, Jakob W, Marienhagen J, Zrenner E and Gabel V P 2000 Subretinal implantation of electrodes for acute in vivo stimulation of the retina to evoke cortical responses in minipig *Invest. Ophthalmol. Vis. Sci.* **41** S102–S102
[14] Palanker D, Vankov A, Mirkin M V, Fishman H A, Blumenkranz M S and Marmor M F 2004 Physical constraints on the design of a high-resolution electronic retinal prosthesis *IEEE Trans. Biomed. Eng.* submitted
[15] Palanker D, Huie P, Vankov A, Freyvert Y, Fishman H A, Marmor M F and Blumenkranz M S 2004 *Attracting Retinal Cells to Electrodes for High-Resolution Stimulation* vol 5314 (San Jose, CA: SPIE)
[16] Palanker D, Huie P, Vankov A, Aramant R, Seiler M, Fishman H, Marmor M and Blumenkranz M 2004 Migration of retinal cells through a perforated membrane: implications for a high-resolution prosthesis *Invest. Ophthalmol. Vis. Sci.* **45** 3266–70
[17] Eckmiller R, Hünermann R and Becker M 1999 Exploration of a dialog-based tunable retina encoder for retina implants *Neurocomputing* **26–27** 1005–11
[18] Coppola D and Purves D 1996 The extraordinarily rapid disappearance of entopic images *Proc. Natl Acad. Sci. USA* **93** 8001–4
[19] Chow A Y, Pardue M T, Perlman J I, Ball S L, Chow V Y, Hetling J R, Peyman G A, Liang C, Stubbs E B Jr and Peachey N S 2002 Subretinal implantation of semiconductor-based photodiodes: durability of novel implant designs *J. Rehabil. Res. Dev.* **39** 313–21
[20] Zrenner E 2002 The subretinal implant: Can microphotodiode arrays replace degenerated retinal photoreceptors to restore vision? *Ophthalmologica* **216** 8–20
[21] Zenisek D, Henry D, Studholme K, Yazulla S and Matthews G 2001 Voltage-dependent sodium channels are expressed in nonspiking retinal bipolar neurons *J. Neurosci.* **21** 4543–50
[22] Pan Z H and Hu H J 2000 Voltage-dependent Na+ currents in mammalian retinal cone bipolar cells *J. Neurophysiol.* **84** 2564–71
[23] Mennerick S and Matthews G 1996 Ultrafast exocytosis elicited by calcium current in synaptic terminals of retinal bipolar neurons *Neuron* **17** 1241–9
[24] Mennerick S and Matthews G 1998 Rapid calcium-current kinetics in synaptic terminals of goldfish retinal bipolar neurons *Vis. Neurosci.* **15** 1051–6
[25] Matthews G 1999 Synaptic mechanisms of bipolar cell terminals *Vis. Res.* **39** 2469–76
[26] Greenberg R J, Velte T J, Humayun M S, Scarlatis G N and de Juan E 1999 A computational model of electrical stimulation of the retinal ganglion cell *IEEE Trans. Biomed. Eng.* **46** 505–14
[27] Jensen R J, Rizzo J F, Ziv O R III, Grumet A and Wyatt J 2003 Thresholds for activation of rabbit retinal ganglion cells with an ultrafine, extracellular microelectrode *Invest. Ophthalmol. Vis. Sci.* **44** 3533–43
[28] Coburn B 1989 Neural modeling in electrical-stimulation *Crit. Rev. Biomed. Eng.* **17** 133–78
[29] Dowling J E 1987 *The Retina: An Approachable Part of the Brain* (Cambridge, MA: Belknap Press of Harvard University Press)
[30] Levitan I B and Kaczmarek L K 1997 *The Neuron: Cell and Molecular Biology* (New York: Oxford University Press)
[31] Yang X L and Wu S M 1997 Response sensitivity and voltage gain of the rod and cone bipolar cell synapses in dark-adapted tiger salamander retina *J. Neurophysiol.* **78** 2662–73
[32] Berntson A and Taylor W R 2000 Response characteristics and receptive field widths of on-bipolar cells in the mouse retina *J. Physiol., London* **524** 879–89
[33] Hibino M, Itoh H and Kinosita K 1993 Time courses of cell electroporation as revealed by submicrosecond imaging of transmembrane potential *Biophys. J.* **64** 1789–800
[34] Hesse L, Schanze T, Wilms M and Eger M 2000 Implantation of retina stimulation electrodes and recording of electrical stimulation responses in the visual cortex of the cat *Graef Arch. Clin. Exp.* **238** 840–5
[35] Schwahn H N, Gekeler F, Kohler K, Kobuch K, Sachs H G, Schulmeyer F, Jakob W, Gabel V P and Zrenner E 2001 Studies on the feasibility of a subretinal visual prosthesis: data from Yucatan micropig and rabbit *Graef Arch. Clin. Exp.* **239** 961–7
[36] Mierisch A M, Taylor S R and Celli V 2003 Understanding the degradation of organic coatings through local electrochemical impedance methods: II. Modeling and experimental results of normal field variations above disk electrodes *J. Electrochem. Soc.* **150** B309–B315
[37] Greenberg R J, Humayun M S and de Juan E 1997 Electrical stimulation pulse-width determines the target cell in the frog and human retina *Invest. Ophthalmol. Vis. Sci.* **38** 183–183
[38] Malmivuo J and Plonsey R 1995 *Subthreshold Membrane Phenomena. Bioelectromagnetism* (New York: Oxford University Press) pp 44–65
[39] Bard A J and Faulkner L R 2001 *Electrochemical Methods: Fundamentals and Applications* (New York: Wiley)
[40] Bron M, Radnik J, Fieber-Erdmann M, Bogdanoff P and Fiechter S 2002 EXAFS, XPS and electrochemical studies on oxygen reduction catalysts obtained by heat treatment of iron phenanthroline complexes supported on high surface area carbon black *J. Electroanal. Chem.* **535** 113–9
[41] Weiland J D, Anderson D J and Humayun M S 2002 In vitro electrical properties for iridium oxide versus titanium nitride stimulating electrodes *IEEE Trans. Biomed. Eng.* **49** 1574–9
[42] Hammerle H, Kobuch K, Kohler K, Nisch W, Sachs H and Stelzle M 2002 Biostability of micro-photodiode arrays for subretinal implantation *Biomaterials* **23** 797–804
[43] Guenther E, Troger B, Schlosshauer B and Zrenner E 1999 Long-term survival of retinal cell cultures on retinal implant materials *Vis. Res.* **39** 3988–94
[44] Klein J D, Clauson S L and Cogan S F 1989 Morphology and charge capacity of sputtered iridium oxide-films *J. Vac. Sci. Technol.* A **7** 3043–7
[45] Meyer R D, Cogan S E, Nguyen T H and Rauh R D 2001 Electrodeposited iridium oxide for neural stimulation and recording electrodes. *IEEE Trans. Neuro. Syst. Rehabil.* **9** 2–11
[46] Mozota J and Conway B E 1983 Surface and bulk processes at oxidized iridium electrodes: 1. Monolayer stage and transition to reversible multilayer oxide film behavior *Electrochim. Acta* **28** 1–8
[47] Robblee L S, Mchardy J, Marston J M and Brummer S B 1980 Electrical-stimulation with Pt electrodes: 5. The effect of protein on Pt dissolution *Biomaterials* **1** 135–9
[48] Rose T L and Robblee L S 1990 Electrical-stimulation with Pt electrodes: 8. Electrochemically safe charge injection limits with 0.2 Ms pulses *IEEE Trans. Biomed. Eng.* **37** 1118–20

[49] Rohsenow W M, Hartnett J P and Gani E N 1985 *Handbook of Heat Transfer Fundamentals* 2nd edn (New York: McGraw-Hill) chapter 4 p 164
[50] Baruth O, Neumann D and Eckmiller R E 2003 Pattern encoding and data encryption in learning retina implants *Invest. Ophthalmol. Vis. Sci.* **44** (Suppl. 2) U701–U701
[51] Skavenski A A, Hansen R M, Steinman R M and Winterson B J 1979 Quality of retinal image stabilization during small natural and artificial body rotations in man *Vis. Res.* **19** 675–83
[52] Blumenkranz M S, Ophir A, Claflin A J and Hajek A 1982 Fluorouracil for the treatment of massive periretinal proliferation *Am. J. Ophthalmol.* **94** 458–67
[53] Olveczky B P, Baccus S A and Meister M 2003 Segregation of object and background motion in the retina *Nature* **423** 401–8
[54] Baccus S A and Meister M 2002 Fast and slow contrast adaptation in retinal circuitry *Neuron* **36** 909–19
[55] Meister M, Pine J and Baylor D A 1994 Multi-neuronal signals from the retina—acquisition and analysis *J. Neurosci. Methods* **51** 95–106